AGU ADVANCING EARTH AND SPACE SCIENCE

JGR Earth Surface

RESEARCH ARTICLE
10.1029/2022JF006775

Predicting Subsurface Architecture From Surface Channel Networks in the Bengal Delta

Zhongyuan Xu[1,2], Mahfuzur R. Khan[3], Kazi Matin Ahmed[3], Anwar Zahid[4], Jayaram Hariharan[5], Paola Passalacqua[5], Elisabeth Steel[6], Austin Chadwick[7], Chris Paola[7], Steven L. Goodbred Jr.[8], Anner Paldor[2], and Holly A. Michael[2,9]

[1]Faculty of Geosciences and Environmental Engineering, Southwest Jiaotong University, Chengdu, China, [2]Department of Earth Sciences, University of Delaware, Newark, DE, USA, [3]Department of Geology, University of Dhaka, Dhaka, Bangladesh, [4]Bangladesh Water Development Board, Dhaka, Bangladesh, [5]Department of Civil, Architectural and Environmental Engineering, Center for Water and the Environment, University of Texas at Austin, Austin, TX, USA, [6]Department of Geological Sciences and Geological Engineering, Queen's University, Kingston, ON, Canada, [7]St. Anthony Falls Laboratory and Department of Earth and Environmental Sciences, University of Minnesota, Minneapolis, MN, USA, [8]Department of Earth and Environmental Sciences, Vanderbilt University, Nashville, TN, USA, [9]Department of Civil and Environmental Engineering, University of Delaware, Newark, DE, USA

Key Points:

- We demonstrate a novel approach that harnesses land surface characteristics to inform groundwater modeling in deltas
- The subsurface lithologic data of an active delta is more consistent with surface features than that of an inactive delta
- Incorporation of surface information can improve the prediction of contaminant transport in aquifers

Supporting Information:

Supporting Information may be found in the online version of this article.

Correspondence to:

H. A. Michael,
hmichael@udel.edu

Citation:

Xu, Z., Khan, M. R., Ahmed, K. M., Zahid, A., Hariharan, J., Passalacqua, P., et al. (2023). Predicting subsurface architecture from surface channel networks in the Bengal Delta. *Journal of Geophysical Research: Earth Surface*, *128*, e2022JF006775. https://doi.org/10.1029/2022JF006775

Received 25 MAY 2022
Accepted 22 FEB 2023

Abstract Groundwater is the primary source of water in the Bengal Delta but contamination threatens this vital resource. In deltaic environments, heterogeneous sedimentary architecture controls groundwater flow; therefore, characterizing subsurface structure is a critical step in predicting groundwater contamination. Here, we show that surface information can improve the characterization of the nature and geometry of subsurface features, thus improving the predictions of groundwater flow. We selected three locations in the Bengal Delta with distinct surface river network characteristics—the lower delta with straighter tidal channels, the mid-delta with meandering and braided channels, and the inactive delta with transitional sinuous channels. We used surface information, including channel widths, depths, and sinuosity, to create models of the subsurface with object-based geostatistical simulations. We collected an extensive set of lithologic data and filled in gaps with newly drilled boreholes. Our results show that densely distributed lithologic data from active lower and mid-delta are consistent with the object-based models generated from surface information. In the inactive delta, metrics from object-based models derived from surface geometries are not consistent with subsurface data. We further simulated groundwater flow and solute transport through the object-based models and compared these with simulated flow through lithologic models based only on variograms. Substantial differences in flow and transport through the different geologic models show that geometric structure derived from surface information strongly influences groundwater flow and solute transport. Land surface features in active deltas are therefore a valuable source of information for improving the evaluation of groundwater vulnerability to contamination.

Plain Language Summary The structure of groundwater aquifers affects how groundwater and contaminants move through them. In deltas, dynamic river networks are responsible for depositing sediments that ultimately form subsurface aquifers. Therefore, the characteristics of the surface river channel network should provide information about the structure of the subsurface. We tested this idea using a large set of sedimentary data from the Bengal Basin. We created models of the subsurface based on the surface network and showed that the subsurface data reflect the model characteristics in deltas that are actively depositing sediment. Using these subsurface models as input for groundwater flow models, we showed that incorporating this surface information is important for being able to predict how contaminants move in groundwater.

1. Introduction

Deltas are densely populated areas with high socioeconomic, agricultural, and environmental value (Seto, 2011; Syvitski & Saito, 2007; Szabo et al., 2016). Groundwater is the major freshwater resource in deltas and is vulnerable to multiple threats, including sea-level rise, overpumping, and extreme climate conditions (Ayers et al., 2016; Hosono et al., 2011; Michael & Voss, 2008; van Engelen et al., 2021). In the Bengal Delta, more than 150 million inhabitants rely on groundwater as their primary source of water due to its accessibility and lower risk of microbial contamination compared to surface water (Bangladesh Bureau of Statistics, 2011). However, 27.5 million people are drinking groundwater with high levels of geogenic arsenic in the shallow

Accepted Manuscript
Version of Record at: https://doi.org/10.1029/2022JF006775

(<~100m) Holocene aquifer (Bangladesh Bureau of Statistics, 2021) and nearly 20 million people are at high risk of drinking groundwater contaminated by saltwater intrusion (Rasheed et al., 2016; Shammi et al., 2019). Despite the existence of an extensive set of lithologic data, knowledge of the stratigraphic architecture of the aquifer is limited. This is due to the complexity of heterogeneous sediments, the connectedness of which is critical for understanding recharge, flow, and transport (i.e., Hoque et al., 2014; McArthur et al., 2011; Khan et al., 2016; Mozumder et al., 2020). Our motivation here is to investigate whether incorporating information from the delta surface could address some of these issues and improve models of subsurface connectedness and thus predictions of groundwater contamination risks in deltaic aquifers (Hariharan et al., 2021; Xu et al., 2021).

It is clear that subsurface heterogeneity strongly influences groundwater flow and solute transport in the Bengal Delta; groundwater vulnerability to contamination is underestimated if heterogeneity is not explicitly considered (Khan et al., 2016; Michael & Khan, 2016). Van Geen et al. (2008) suggested that rapid groundwater flow through aquifers with sandy connections to the surface reduces arsenic concentrations compared to aquifer zones beneath low-permeability surface layers. Groundwater arsenic concentrations are affected by the presence of paleosols, with paleo-channel and paleo-interfluvial sediments hosting arsenic-polluted and arsenic-free groundwater, respectively (Hoque et al., 2012; McArthur et al., 2011). Hoque et al. (2017) explained the variable subsurface arsenic distribution by considering aquifers composed of sand and discontinuous silt-clay layers. Recent studies show that clay layers have a substantial effect on arsenic transport from Holocene to pre-Holocene aquifer strata (Hoque et al., 2017; Khan et al., 2019; Mihajlov et al., 2020; Mozumder et al., 2020). Subsurface heterogeneities also impact salinity distributions. Saline water infiltrates into groundwater from salinized tidal channels (Bricheno et al., 2021) and brine ponds (Ayers et al., 2016), and paleo-brackish estuarine water is slowly transported into the aquifers from muddy sediments (Ayers et al., 2016; Worland et al., 2015). Saline water infiltration from the surface was shown to be limited by low-permeability mud deposits (Tasich, 2012), and Ayers et al. (2016) showed that discontinuous silt-mud layers cause highly variable salinity distributions in coastal groundwater. Naus et al. (2019) found that paleo-hydrologic processes control salinity under thick surface clay layers, and modern processes influence salinity under thin surface clay layers. Several large tidal channels are deeper than the clay layers, acting as conduits for vertical saline (dry season) or fresh (wet season) water recharge (Ayers et al., 2016). Small-scale heterogeneity such as crab burrows can also have a potential effect on contaminant transport, creating flow conduits by penetrating pond-bottom clay (Stahl et al., 2014).

Although the importance of deltaic heterogeneity for groundwater pollution has been demonstrated, representation of litho-facies architecture is difficult due to scarce lithologic data. Recent studies have shown that linking surface morphology and subsurface lithology has the potential to improve the prediction of groundwater contamination (Hariharan et al., 2021; Xu et al., 2021, 2022; van Dijk et al., 2016a). The fluvial sedimentary processes that created the shallow subsurface should be similar to current fluvial processes if the time span between them is relatively short (Liang et al., 2016; Miall, 2014; Rongier et al., 2017). Researchers have quantitatively considered the architecture of fluvial features, such as channels, point bars, crevasse-splays, and their migration processes in trying to understand reservoir heterogeneity and connectivity (Colombera & Mountney, 2021; Colombera et al., 2017; Donselaar & Overeem, 2008; Gouw & Hijma, 2022). Furthermore, the influence of geomorphologic processes on fluvial deposits is central to process-based reservoir models (Grimaud et al., 2022; Liang et al., 2015), rule-based methods (Colombera et al., 2018), and random-walk simulations (van Dijk et al., 2016b).

The primary objective of this work is to determine whether geomorphological characteristics of the land surface can provide useful information to improve models of delta subsurface architecture. A secondary objective is to determine how such information impacts the prediction of groundwater flow and solute transport relative to even very densely distributed lithologic data. We approach these objectives by creating object-based geostatistical models of subsurface structure using information from the modern surface-channel network at three locations in the Bengal Delta. Using a set of statistical metrics, we compare the 3D geometrical properties of the object-based simulations with a dense network of subsurface lithology data derived from well logs. We then carry out simulations of groundwater flow through the object-based subsurface models and a set of variogram-based subsurface models derived from the field observations. We show that incorporation of surface features substantially alters predictions of contaminant transport in groundwater. Our findings demonstrate that incorporating surface information can substantially improve models of aquifer heterogeneity.

Accepted Manuscript
Version of Record at: https://doi.org/10.1029/2022JF006775

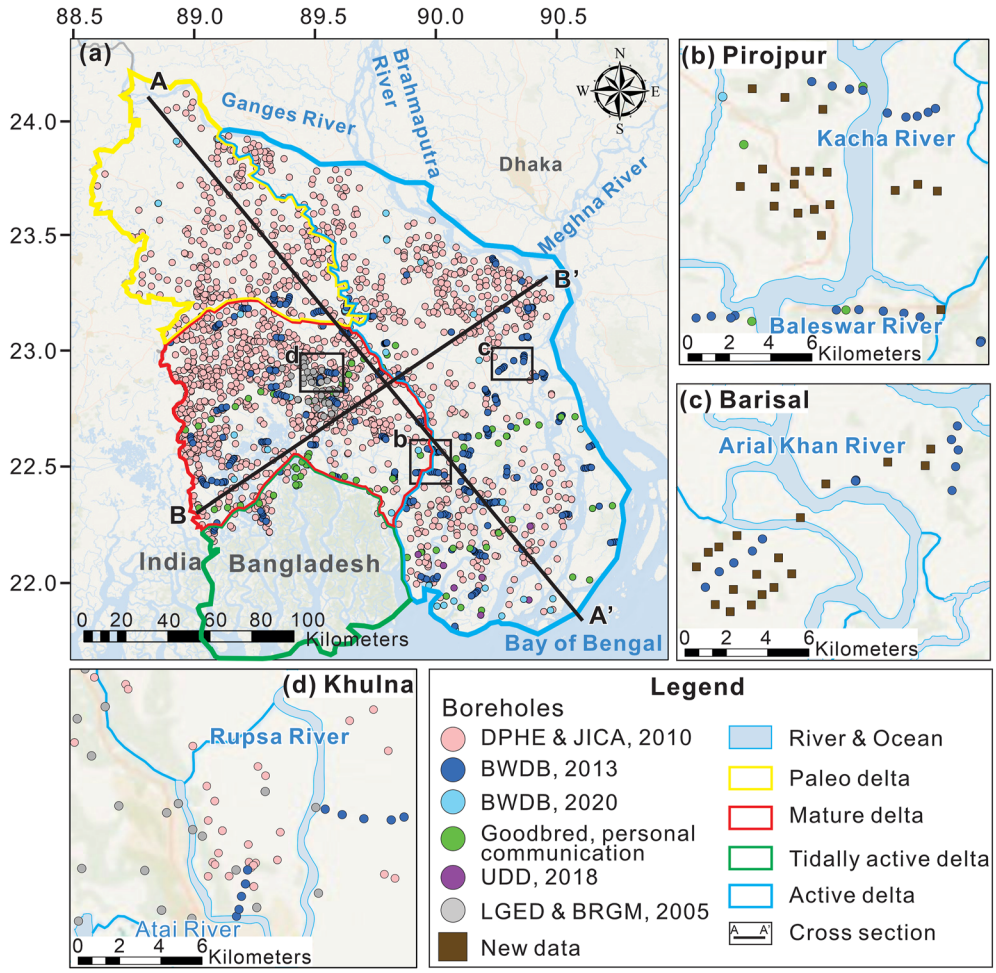

Figure 1. Geomorphic regions and boreholes in the study area. (a) Borehole locations and data sources (Table S1 in Supporting Information S1). The regional study sites are (b) Pirojpur, (c) Barisal, and (d) Khulna. The corresponding Google Earth map is shown in Figure S4 in Supporting Information S1. Plots of borehole data on cross sections are shown in Figures S1b and S1c in Supporting Information S1.

2. Stratigraphic Setting and Context of the Study Area

The Bengal Delta is situated in a remnant ocean basin where about 20 km thick Himalayan sediments have been deposited in deep marine to fluvio-deltaic settings since the Early Miocene (Alam et al., 2003; Atker et al., 2016; Goodbred & Kuehl, 2000) (Figure 1; Figure S1 in Supporting Information S1). The modern Ganges and Brahmaputra Rivers (Figure S1 in Supporting Information S1) contribute to delta development through annual transport of nearly one billion tons of sediment from the Himalayas (Goodbred & Kuehl, 2000; Milliman & Syvitski, 1992; Wilson & Goodbred, 2015). Development of the modern delta began after the Younger Dryas (~12 ka), earlier than other deltas in the world due to a doubling of the average sediment load delivered under a strengthened monsoon and increased river discharge (Goodbred & Kuehl, 2000). Nearly 60% of Holocene delta sediments are deposited during this 8–12 ka period under the dominant influence of riverine channel processes, with limited preservation of fine-grained fluvial or marine sediments (Wilson & Goodbred, 2015). From mid-Holocene to present, moderated rates of sediment delivery and sea-level rise support a more balanced interplay between fluvial and tidal processes, resulting in greater preservation of fine-grained floodplain and coastal deposits (Goodbred et al., 2003).

Since the mid-Holocene, avulsion and migration of the Ganges and Brahmaputra river channels effectively disperse sediment across the Bengal basin to compensate for subsidence and sea-level rise. Field evidence suggests ~4 major avulsions for each river in the last 6–8 kyrs, suggesting an avulsion period of 1–2 kyrs (Allison et al., 2003;

Accepted Manuscript
Version of Record at: https://doi.org/10.1029/2022JF006775

Pickering et al., 2014). This avulsion timescale is consistent with the development of channel super-elevation and compensational stacking behavior (Reitz et al., 2015), which influence the sand stacking patterns and amalgamated sand bodies formed in the upper delta (Bhattacharya, 2011; Miall, 2014; Rongier et al., 2017). The provenance signatures of sandy channel deposits preserved in the delta over this time also suggest that the two rivers were not confluent through most of the Holocene (Goodbred et al., 2014), making the present channel configuration unique to the past 200 years. In the upper delta, the channels are predominantly braided and sustain rapid channel aggradation and migration, favoring the preservation of coarse-grained channel deposits (Pickering et al., 2014; Wilson & Goodbred, 2015). In the lower delta, almost all flow and sediments pass through bifurcating channels of the Meghna estuary and form a vast turbid river plume on the inner shelf (Atker et al., 2016; Barua et al., 1994). Flood-dominant tides then advect suspended river-plume sediments back onshore to form a vast muddy tidal delta plain sustained by a dense network of channels and intertidal platform (Allison et al., 1998; Rogers et al., 2013). The resulting stratigraphy is mud-dominated and faces higher rates of subsidence due to natural compaction and exacerbated by anthropogenic activities (Allison et al., 2003; Atker et al., 2016; Auerbach et al., 2015; Grall et al., 2018; Rogers et al., 2013; Steckler et al., 2022). Recent studies (Islam & Gnauck, 2008; Passalacqua et al., 2013) divided the study area into four geomorphic regions: active, tidally active, mature, and paleo-delta (Figure 1a). Active and tidally active regions are those where delta building is currently ongoing, but the former is dominated by fluvial processes and the latter is dominated by tidal processes. In contrast, deltaic sedimentation in the mature and paleo-delta regions is sustained only by ephemeral distributaries, with accretion rates only ∼1/10 of those in the active delta (Goodbred & Kuehl, 1998).

In this study, we chose three small-scale sites in which to investigate surface-subsurface translation. Barisal (Figure 1c) is in the upper active delta, where sediment deposition is mainly controlled by the fluvial system and tides. Khulna (Figure 1d) is in the mature (inactive) delta, with a series of small and shallow rivers that have a slow deposition rate under current conditions. Pirojpur (Figure 1b) is at the boundary of the lower active and mature delta. However, we consider Pirojpur to lie in the lower active delta for three reasons: (a) the location of the boundary is approximate (Islam & Gnauck, 2008); (b) the Kacha River is a major local river running through the Pirojpur site, causing an active sedimentary environment; and (c) frequent sand-mud transitions in the existing borehole records indicate active deposition and channel migration.

3. Methods

3.1. Subsurface Data Acquisition

We compiled lithology from 2,813 boreholes from various databases and reports in the study area (Figure 1a, sources are listed in Table S1 in Supporting Information S1). These boreholes were drilled and recorded by geologists and field engineers across Bangladesh. The sampling interval varied from 1.5 to 3 m among different sources.

Within that data set, we extracted data from the three study areas discussed above as representative of various morphologies within the delta: Pirojpur, Barisal, and Khulna (Figure 1). In Pirojpur and Barisal, data density was not sufficient for our study, so we drilled 37 new boreholes (brown squares Figures 1b and 1c). The new borehole depths ranged 50–60 m and the sampling interval was 1 m to ensure high resolution (Xu, 2022). The locations of the new boreholes were chosen to fill in gaps between the existing data locations and to create telescoping scales of spatial resolution. At both sites, the Bangladesh Water Development Board (BWDB, 2013) had drilled two existing transects across the river (blue circles in Figures 1b and 1c). Thus, we arranged most of the new boreholes between and around these transects (Figures 1b and 1c). No new data were collected at Khulna (Figure 1d) because its existing lithologic data (57 boreholes) are densely distributed enough for our analysis.

3.2. Subsurface Data Analysis

The lithological characterization was visually performed by drillers on site. To minimize errors arising from subjective interpretation of different drillers, we categorized lithologic data into two easily distinguished groups: sand and mud. Three metrics were quantified in each borehole: *sand fraction*, *maximum sand connection*, and the *number of sand-mud shifts*. *Sand fraction* is the cumulative thickness of sandy intervals divided by the total length of each borehole. *Maximum sand connection* is the thickness of the greatest interval of sand divided by the total length of each borehole, which effectively measures the sand connectivity. The *number of sand-mud shifts*

Accepted Manuscript
Version of Record at: https://doi.org/10.1029/2022JF006775

Table 1
Surface Information in the Three Small-Scale Study Areas

River name	Site	Type	Width (m)	Depth (m)	Direction	Amplitude (m)	Sources
Kacha	Pirojpur	Straight	768–1,168	Max 15	0–3°	600–1,200	BWDB (2011), DevCon-DPM-KPL (2013)
Baleswar	Pirojpur	Straight	44–3,000	7	15°	100–500	Ahmad (2014), BWDB (2011)
Arian Khan	Barisal	Meandering	86–1,940	12	−23°–26°	700–1,500	BWDB (2011)
Kirtankhola	Barisal	Meandering	321–674	Max 30	32°	800–1,500	BWDB (2011), Ghosh (2020)
Atai	Khulna	Meandering	150–360	Max 12.8	9°	300–700	BWDB (2011), JICA (1999)
Rupsa	Khulna	Meandering	322–650	Max 13.2	0°–20°	~400	BWDB (2011), JICA (1999)

Note. Direction: the north-south direction is defined as 0°, clockwise is the positive direction.

reflects the sediment transitions, which are related to depositional processes such as channel migration and tidal effects. We note that *maximum sand connection* and *number of sand-mud shifts* are likely interrelated (larger sand connectivity means fewer shifts), but they are still useful separately because they are indicative of different depositional characteristics.

The drilling method and sampling interval (Table S1 in Supporting Information S1) may influence the metrics calculated from lithologic data. The reverse circulation hand-flapper drilling method was used for the new drillings along with the data from Goodbred (2020) (green circles and brown squares in Figure 1). The other boreholes were drilled by direct circulation rotary wash boring. Thin clay layers are more easily identified using the hand-flapper method than the rotary wash method; thus, clay may be underrepresented in the rotary-wash data. In addition, the sampling interval may influence the statistical results since 1 m-interval sampling provides higher resolution of sand-mud distributions in the vertical direction than coarser intervals. A test was applied to investigate the influence of the drilling method and sampling interval on the lithologic metrics at the Pirojpur and Barisal sites (Text S1 in Supporting Information S1). We found that sampling interval influences the lithologic metrics, especially the *number of sand-mud shifts*, at the Pirojpur site but not at the Barisal site. In order to ensure enough data in the statistical analysis, all the data, both high-resolution and low-resolution, were used in this work. However, in the large-scale analysis, we only considered 3 m-interval boreholes in the calculation of sand-mud shifts since the resolution of the sampling interval strongly influences this metric. For example, 1.5 m-interval sampling may record more sand-mud shifts than 3 m-interval sampling (Text S1 in Supporting Information S1). We used all data in the calculation of sand fraction since sampling interval insignificantly influences it. These three metrics performed well in linking surface properties, subsurface structure, and groundwater behavior of synthetic models (Hariharan et al., 2021; Xu et al., 2021).

3.3. Surface Data Acquisition and Analysis

We characterized surface features by analyzing rivers in the regions around the three study sites (Table 1). Two nearby rivers for each site were selected for quantifying surface characteristics. River depths were collected from multiple sources (Table 1). The river widths were obtained from Google Earth (Figure S4 in Supporting Information S1) by selecting only the width of river reaches around the study sites. We measured the river orientations and amplitudes of river bends on Google Earth within the study sites (in the boxes of Figure 1). The river orientations in the study regions were approximated, ignoring small variations in the directions of the different reaches. Multiple rivers show different orientations in the Barisal and Khulna sites, so a range of values was used (Table 1). We manually identified amplitudes from river bends on Google Earth by measuring the greatest distance from channel bend to a point along a hypothetical straight channel. These parameters were used to define the geobodies used in geostatistical modeling in Section 3.4.

3.4. Geostatistical Methods

We used geostatistical techniques in several different ways to analyze the spatial data and create simulations. At the large scale, sand fraction and the number of sand-mud shifts within the top 100 m for each lithology were interpolated across the delta via Kriging using spherical variograms to fit the data in 2D (Figure S5 in Supporting Information S1).

Accepted Manuscript
Version of Record at: https://doi.org/10.1029/2022JF006775

Table 2
The Parameters of Object-Based Models of Three Small-Scale Regions

		Sinusoid system				Lower-ellipsoid system	
Site	Sand fraction	Width (m)	Depth (m)	Direction (°)	Amplitude (m)	Radius (m)	Thickness (m)
Pirojpur	0.40	(700,1500)	(7,15)	0	(100,500)	(600,1200)	(7,15)
Barisal	0.55	(300,1200)	(12,30)	(−30,30)	(700,1500)	(700,1500)	(12,30)
Khulna	0.55	(200,700)	(5,13)	(−20,20)	(300,700)	(300,700)	(5,13)

Note. These parameters were determined from surface river information in Table 1, Figure 1, and Figure S4 in Supporting Information S1. The dimensions were drawn from uniform distributions across the range of values in parentheses. Direction: the north-south direction is defined as 0°, clockwise is the positive direction.

In the small-scale study sites, we used object-based simulation techniques to create models of the subsurface using parameters (Table 2) from satellite image-derived surface characteristics (Table 1, Figure S4 in Supporting Information S1) and sand proportions derived from lithologic data. Object-based simulation is a method that generates geologic features as mathematical representations of sand objects, such as channel-like or spherical objects, and stochastically places them in the background matrix. These representations allow the geometrical parametrization of geologic heterogeneity and connectivity, such as paleo-channels in fluvial and deep-water systems (Deutsch & Tran, 2002; Deutsch & Wang, 1996; Haldorsen & Lake, 1984; Pyrcz & Deutsch, 2014). We expect that at the local scale of fluvial deposition, preserved subsurface structures may be either sinusoidal (i.e., coarse material deposited in channels with varying sinuosity within a mud matrix) or ellipsoidal (i.e., coarse material deposited as bars or splays within a mud matrix), depending on the nature of deposition. We created sets of models for each site, one with sinusoidal features and one with lower-ellipsoidal features, using the geostatistical software SGeMS (Maharaja, 2008; Remy et al., 2009). For parameters with a range of values, we drew from a uniform probability distribution in the object-based simulation. In the sinusoid object-based simulations (Figure 2a), the widths and thicknesses of sinusoid objects were widths and depths of surface rivers taken from literature values (Table 1) and Google Earth (Section 3.3). The orientation and amplitude of objects were river flow direction and meander amplitude obtained from Google Earth. In the lower-ellipsoid simulations (Figure 2b), the radius of the objects was measured from the amplitudes of river meanders in Google Earth. We did not consider anisotropy of these meanders, so Diameter 1 equals Diameter 2 in this study (Figure 2b). The thicknesses of lower-ellipsoid objects were the depths of the surface rivers obtained from literature. The volume of geobodies relative to the whole system was set as the sand fraction derived from the lithologic data. These objects represent sandy fluvial deposits, while baffles, clay plugs, and other interfluvial deposits are considered part of the mud matrix since they likely have similar low permeability as the mud, relative to sand.

Sand objects were stochastically placed in the mud matrix until the sand proportion was similar to the target proportion. The center-point location of each object was drawn randomly from a uniform distribution. The features of each object were also drawn randomly from uniform distributions with ranges in Table 1. The resulting 3D model constitutes one realization. Ten realizations were generated for each model type (see the test of realization

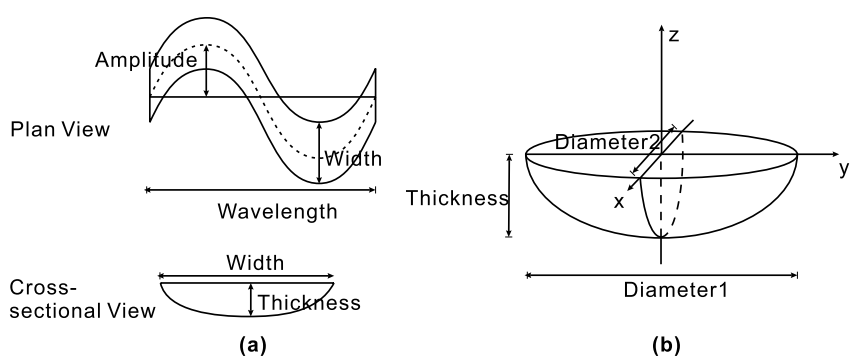

Figure 2. Parameters of an object in the sinusoid model and lower-ellipsoid model. (a) Plan view and cross-sectional view of a sinusoid object. (b) Lower-ellipsoid object. Modified from Maharaja (2008).

Accepted Manuscript
Version of Record at: https://doi.org/10.1029/2022JF006775

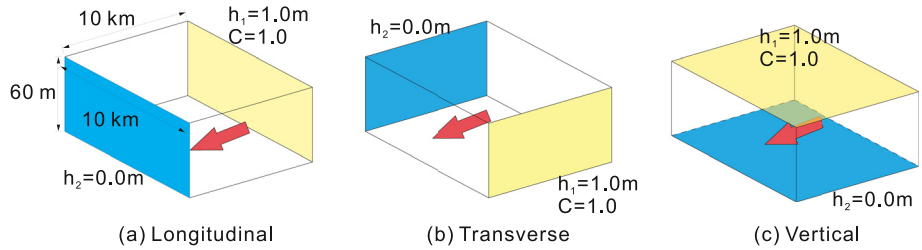

Figure 3. Boundary conditions of (a) longitudinal, (b) transverse, and (c) vertical cases. Yellow face is the higher-head and solute source boundary, blue is the lower-head boundary, and no-color faces are no-flow boundaries. Red arrow in the figure represents the expanding direction of potential geobodies, with an orientation that aligns with longitudinal direction.

number in Text S2 in Supporting Information S1). The size of each model is 10 km × 10 km × 60 m, and the dimension of each discretized cell is 100 m × 100 m × 1 m. To evaluate the model agreement with lithologic data, pseudo-boreholes were placed in each object-based model at the exact location where real boreholes exist in the field (Figure 1). The lithologic metrics (sand fraction, maximum sand connection, and number of sand-mud shifts) and variogram ranges were calculated from these pseudo-boreholes for comparison with field data.

Finally, we used a third geostatistical technique, Sequential Indicator Simulation (SIS), to investigate the importance of including geometric features in flow and transport simulations, rather than just spatial correlations. We compared groundwater flow simulated with the object-based models to that of traditional variogram-based (SIS) models. We generated 10 corresponding models for each group of SIS models as benchmarks. Variogram-based methods depend on the assumption of spatial correlation between two points in space; thus, they do not produce continuous geometric features such as those incorporated with object-based modeling. SIS is a widely used variogram-based method to create 3D models of categorical variables based on spatial correlations and lithologic data (Caers, 2000; Journel & Alabert, 1988; Juang et al., 2004; Seifert & Jensen, 1999). Simulation follows a random sequential path in which the facies probability distribution is drawn from indicator kriging, and the simulated values act as data points for the next location. Unlike the object-based models, the SIS models we used were generated directly using horizontal and vertical variogram models fit to field measurements (Figure S6 in Supporting Information S1). While these models replicate the two-point, variogram-based statistics and the sand/mud proportions of the areas, they are not able to capture the connectivity of geobody features derived from surface characteristics as the object-based models do.

3.5. Groundwater Modeling and Evaluation

The aim of the groundwater modeling was to investigate the flow and solute transport behavior in different stratigraphic geometries. The heterogeneous fields generated by object-based models and corresponding SIS models were used in the groundwater flow and solute transport simulation. We froze the sand fraction at 0.5 (average sand fraction of the three study sites) for all the object-based and SIS models in the groundwater simulations to differentiate the effect of geometry from that of sand content. The other parameters in Table 2 were not changed. The lithologic fields were converted to hydraulic conductivity (K), horizontal K values of sand and mud were 3.17×10^{-4} m/s and 9.06×10^{-8} m/s, respectively. These values were determined from the mean of calibrated hydraulic conductivities in the Bengal Delta (Michael & Khan, 2016); the K of sand in this study is the geometric mean of K of fine sand (3.17×10^{-4} m/s) and medium & coarse sand (3.17×10^{-4} m/s) in Michael and Khan (2016). For both materials, anisotropy (the ratio of horizontal to vertical K) was 10. The porosity was 0.4 for both materials to keep the transport solution consistent, the longitudinal and transverse dispersivity values were 1 and 0.1 m, respectively.

MODFLOW (Harbaugh, 2005) and MT3DMS (Zheng & Wang, 1999) were used to simulate groundwater flow and solute transport, respectively. The size of the groundwater models was 10 km × 10 km × 60 m (100 cells × 100 cells × 60 cells). We considered three directions of hydraulic gradient in this study: longitudinal (in the primary channel direction), transverse, and vertical. The head difference for each of the three cases was 1.0 m, resulting in a hydraulic gradient of 0.0001 for the longitudinal and transverse directions, and 0.167 for the vertical direction (Figure 3). All the flow simulations were steady-state. Concentration of contaminant was assigned as 1.0 in each upstream face in the MT3DMS simulations, and the initial concentration of the whole model was

Accepted Manuscript
Version of Record at: https://doi.org/10.1029/2022JF006775

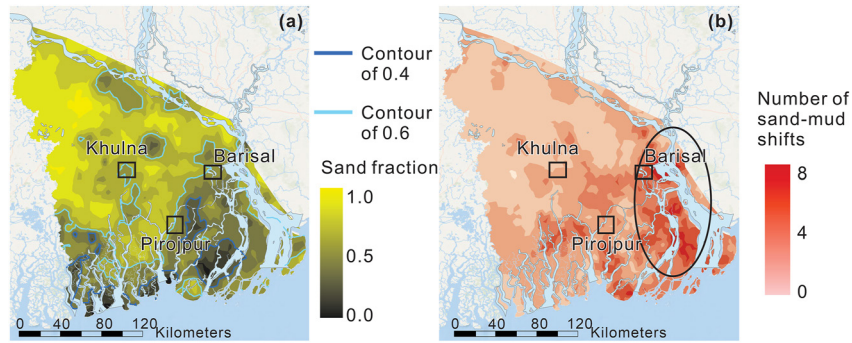

Figure 4. Sand fraction distribution (a) and number of sand-mud shifts (b) across the Bengal delta. The area within the black circle in panel (b) is a zone with frequent sand-mud shifts. The black boxes in both panels are the three small-scale study sites.

zero. These directions may represent horizontal seawater intrusion (longitudinal and transverse directions) and downward migration of salt or arsenic in the vertical direction, neglecting variable density and reactivity. We note that these conditions are simplified, since a patchy distribution of elevated concentrations exists throughout the Holocene aquifer. However, some research suggests that arsenic is released at or near land surface (e.g., Neumann et al., 2010; Pathak et al., 2022; Polizzotto et al., 2008), and these simplified boundary conditions allow direct comparison of the influence of heterogeneity on solute transport.

We used five metrics to evaluate the flow and transport behavior. The first metric is *effective hydraulic conductivity* (K_{eff}), calculated according to Darcy's law by simulating flow through the model in each direction. It represents the overall flow behavior in the model. *Contaminated volume* is the volume of the model where concentrations after 3,000 simulated years were greater than 0.0143 (the drinking water salinity standard 0.5 g/L (EPA, 2009) divided by seawater concentration of 35 g/L) in the longitudinal and transverse directions. *Contaminated volume* mainly measures how much of the aquifer is affected by contamination. *Farthest contaminant extent* is the farthest location of the 0.0143 concentration contour in the longitudinal and transverse directions (measured from the C = 1 boundary), which measures fast solute transport by horizontal sand connections. *Contaminated area at depth* 30 m and *Contaminated area at depth* 60 m are the area of concentration greater than 0.1 divided by the total planar area at depths of 30 and 60 m for vertical solute transport after the 300-year simulation. Both metrics assess vertical contaminant transport affected by sand stacking patterns.

4. Results

4.1. Large-Scale Analysis

We interpolated sand content and sand-mud shifts calculated from 2813 wells in the upper 100 m across the Bengal Delta. In the Kriging interpolation, the range and sill for sand fraction are 1.6 km and 0.04, respectively, and for the sand-mud shift interpolation, the range and sill are 0.6 km and 2.8, respectively (see Figure S5 in Supporting Information S1). Sand content is spatially variable but tends to decrease downstream (Figure 4a). Most of the active southeast delta is less than 60% sand, and several large patches contain less than 40% sand. The seaward active delta has more sand-mud shifts than the upper delta, particularly in areas near the Meghna River and Estuary (Figure 4b, circled in black).

4.2. Site-Scale Analysis

The sand fractions of Pirojpur, Barisal, and Khulna are 0.43, 0.55, 0.53, respectively, and the number of shifts of the three sites are 4.2, 3.8, and 2.9, respectively (Figure 4b), reflecting differences in their depositional environments. Detailed results of each subregion are given in subsequent sections.

4.2.1. Pirojpur Site

The sediment distribution at the Pirojpur site as determined from 44 boreholes (19 newly collected and 25 existing) is summarized as a fence diagram and cross-sections in Figure S8 in Supporting Information S1. The eastern

Accepted Manuscript
Version of Record at: https://doi.org/10.1029/2022JF006775

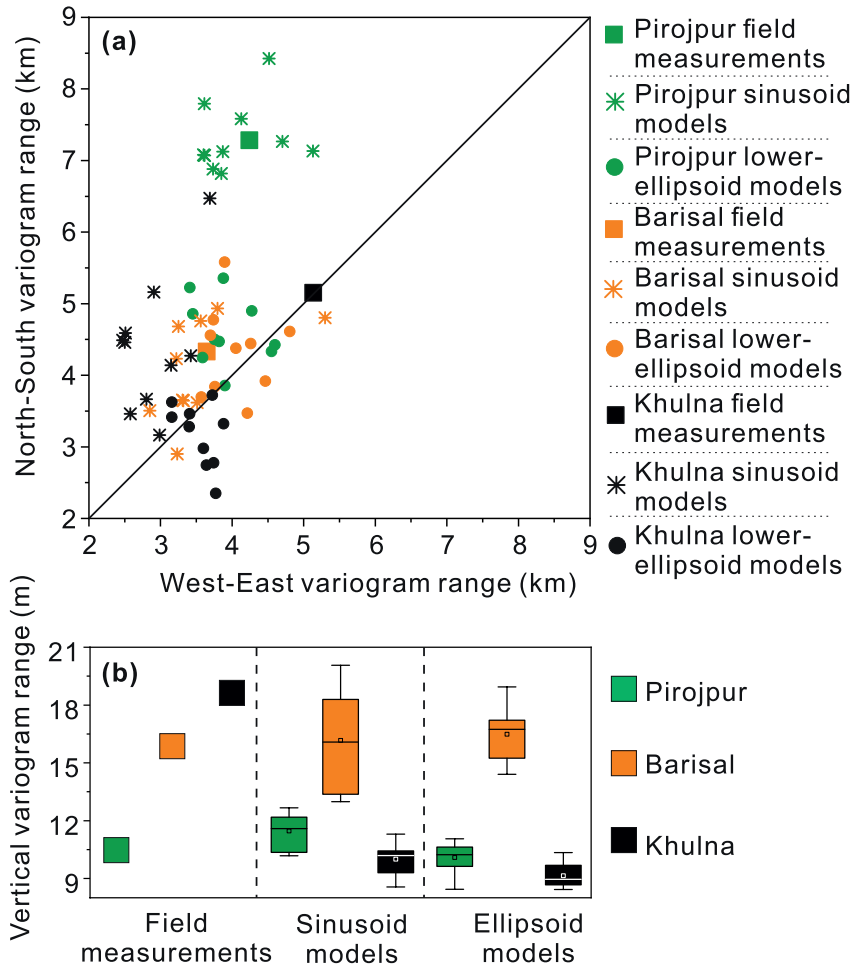

Figure 5. Variogram ranges of field measurement and object-based models in Pirojpur, Barisal, and Khulna. (a) Horizontal variogram ranges, including north-south direction and west-east direction. (b) Vertical variogram ranges. Please see the variogram model of three sites in Figure S6 in Supporting Information S1.

part of the area tends to be more mud-dominated than the western part, though data are sparse in some areas. The denser data in the center of the study site indicate that sand bodies are more extensive in the NS direction (Figure S8 in Supporting Information S1), following the river orientation. This directionality is also evident in the variogram ranges, which have a value of ~7 km in the north-south direction, and ~4 km in the east-west direction (Figure 5a). The vertical variogram range is ~10 m at this site (Figure 5b).

The sand fraction, maximum sand connection, and number of sand-mud shifts of the sinusoid and lower-ellipsoid object-based models derived from surface features (Figures 6a and 6b) are very similar to each other and are not significantly different from those of the field data (Table 3). The vertical variogram ranges of the sinusoid models are slightly higher than the lower-ellipsoid models, and both models yield variogram ranges that span the vertical variogram range of the field data (Figure 5b). For the Pirojpur site, horizontal variograms of the sinusoid models display strong anisotropy, as the north-south variogram ranges are 6.5–8.5 km, whereas the east-west ranges are 3.5–5.0 km (green stars in Figure 5a). These ranges are consistent with the field measurements (green square in Figure 5a). Conversely, the lower-ellipsoid systems show horizontal variogram ranges that are nearly isotropic and are less consistent with field results (green circles in Figure 5a). Therefore, these results indicate that the channelized conceptual model derived from surface information is more representative of the real system than the lower-ellipsoid model for the Pirojpur site.

4.2.2. Barisal Site

We used 29 boreholes to reveal the sediment distribution at the Barisal site, including 18 newly drilled and 11 existing (BWDB, 2013). The data cluster on the southwest side of the site (Figure S9b in Supporting Information S1)

Accepted Manuscript
Version of Record at: https://doi.org/10.1029/2022JF006775

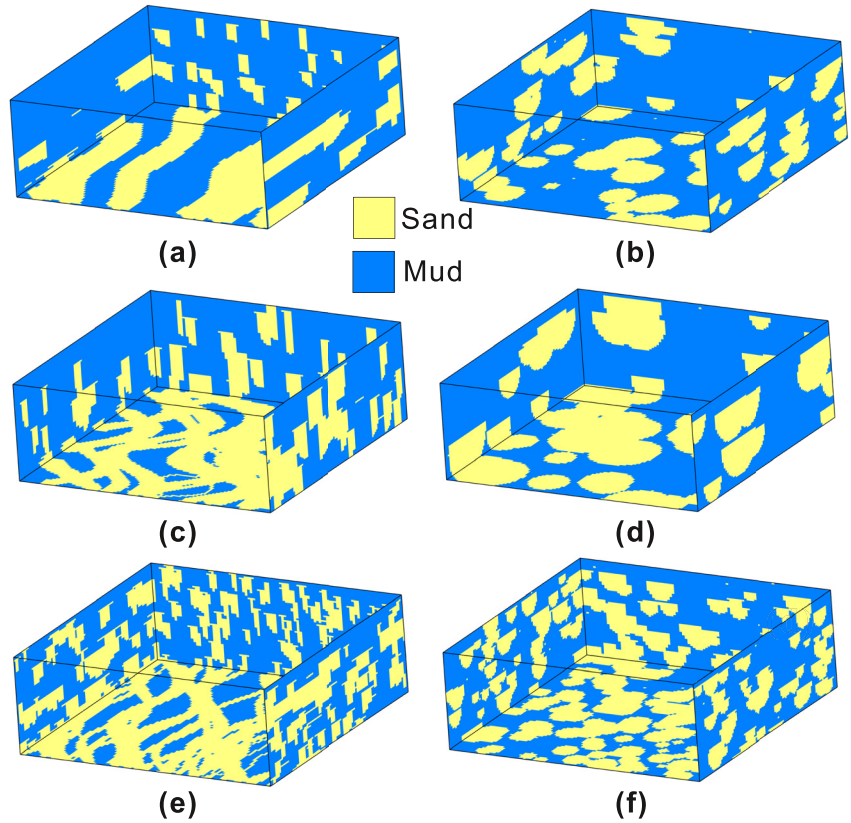

Figure 6. Object-based models simulated using surface feature statistics. Sinusoid (a) and lower-ellipsoid (b) models for Pirojpur site; sinusoid (c) and lower-ellipsoid (d) models for Barisal site; and sinusoid (e) and lower-ellipsoid (f) models for Khulna site.

shows a sand geobody that spans the vertical section with some thin mud layers in the middle. This sand geobody gradually pinches out to the west and east. The northeast group of boreholes shows discontinuous geobodies (Figure S9c in Supporting Information S1). The horizontal variogram in the Barisal site presents a weaker anisotropy than the Pirojpur site, as the north-south variogram range in Barisal is 4.3 km and the west-east range is 3.6 km (Figure 5a). The vertical variogram suggests that geobodies are thicker than at the Pirojpur site, with a range of ~16 m (Figure 5b).

Table 3
Statistical Test Data for Metrics Calculated From Field Measurements and Object-Based Models

Site	Metrics	Sinusoid system	Lower-ellipsoid system
Pirojpur	Sand fraction	8.9×10^{-1}	9.34×10^{-1}
	Max sand connection	2.2×10^{-1}	3.9×10^{-1}
	Number of sand-mud shifts	8.5×10^{-2}	2.6×10^{-1}
Barisal	Sand fraction	8.7×10^{-1}	9.1×10^{-1}
	Max sand connection	2.6×10^{-1}	1.3×10^{-1}
	Number of sand-mud shifts	2.1×10^{-1}	8.2×10^{-2}
Khulna	Sand fraction	9.4×10^{-1}	7.5×10^{-1}
	Max sand connection	$\mathbf{2.3 \times 10^{-6}}$	$\mathbf{1.6 \times 10^{-6}}$
	Number of sand-mud shifts	$\mathbf{2.3 \times 10^{-22}}$	$\mathbf{3.4 \times 10^{-22}}$

Note. The test statistic (p-value) was calculated with a two-sample t-test. Numbers in bold font indicate significant difference (p-value <0.05). The plots of these metrics are in Figure S7 in Supporting Information S1.

Two object-based models (Table 2) were conceptualized for the Barisal site based on river depth and amplitude (Table 1). Due to river sinuosity (Figure 1c), the sinusoid models of Barisal are more tortuous than Pirojpur, and lower-ellipsoid geobodies are larger (Figures 6c and 6d). Similar to the Pirojpur site, the sand fraction, maximum sand connection, number of sand-mud shifts, and vertical variogram ranges of pseudo boreholes are consistent with those of the field measurements (Figure 5b and Table 3). The horizontal variogram ranges (Figure 5a) show that, unlike the Pirojpur site, both lower-ellipsoid and sinusoid systems correspond with field measurements at the Barisal site.

4.2.3. Khulna Site

The Khulna site, located in the mature (inactive) delta, exhibits a different sediment distribution from other sites based on 56 existing boreholes (BWDB, 2013; DPHE & JICA, 2010; LGED & BRGM, 2005). The field data interpolation is shown in Figure S10 in Supporting Information S1. The

Accepted Manuscript
Version of Record at: https://doi.org/10.1029/2022JF006775

horizontal variograms in the Khulna site are both ~5 km, indicating that sand continuity is nearly isotropic (Figure 5a). The vertical variogram range for Khulna is the greatest of the three sites, ~18 m (Figure 5b).

The results of the object-based models for Khulna show that surface information is insufficient to predict subsurface architecture. Due to smaller rivers (Figure 1d and Table 1), object-based simulations generated smaller features at the Khulna Site (Figures 6e and 6f) with significant discrepancies between the modeled and observed ranges of variograms, both in the vertical (Figure 5b) and horizontal directions (Figure 5a). The maximum sand connection and number of sand-mud shifts of the object-based models are also significantly different from those measured in the field (Table 3). Consequently, the subsurface structure of Khulna is not well predicted by the surface-based information.

4.3. Flow and Transport Simulations

The results of Section 4.2 show that Pirojpur sinusoid models, Barisal sinusoid models, and Barisal ellipsoid models are consistent with field measurements of sand distribution. Therefore, these conceptualizations, along with equivalent SIS models (Figure S11 in Supporting Information S1) for the three study sites were used in the groundwater modeling and the simulated contaminant distributions are shown in Figure S13 in Supporting Information S1. K_{eff}, *Contaminated volume*, *Farthest contaminant extent*, *Contaminated area at depth* 30 m, and *Contaminated area at depth* 60 m show the effect of the geometry of subsurface heterogeneity on groundwater contamination (Figure 7), and therefore the value of surface information for solute transport prediction.

Results show that geobody geometry has a substantial influence on flow behavior (K_{eff}) in the three directions (Figures 7a–7c). In the longitudinal direction, aligned with the channels, the K_{eff} values of the Pirojpur sinusoid models (~12.5 m/d) and Barisal sinusoid models (~10.0 m/d) are much larger than those of the Barisal ellipsoid models (5.3–9.3 with mean of 7.5 m/d). Furthermore, the Pirojpur sinusoid models with straighter channels resulted in a higher K_{eff} than the tortuous channels in the Barisal sinusoid models. The longitudinal K_{eff} of corresponding SIS models shows a similar result: Pirojpur values (~11.7 m/d) are slightly greater than Barisal values (~10.2 m/d); although the differences are small, they are statistically significant. SIS models of Pirojpur have a lower K_{eff} than the object-based models, due to the less connected features in variogram-based distributions. The longitudinal K_{eff} of Barisal SIS models (~10.2 m/d) is not significantly different from the Barisal sinusoid models (~10.0 m/d). This indicates that the tortuous-channel system (BS in Figure 7a) has a similar flow connectivity to the variogram-based distribution (BI in Figure 7a).

In the transverse direction, the K_{eff} of object-based models is lower than the corresponding SIS models because the channel structures that align with the longitudinal direction and the ellipsoid structures limit the sand connectivity in the transverse direction (Figure 7b). Among object-based models, tortuous channels tend to form more connections in the transverse direction. Therefore, Barisal sinusoid models have the largest transverse K_{eff} of 5.4–8.9 with mean 7.7 m/d. The straighter channels of Pirojpur sinusoid models result in connected mud barriers that limit flow in the transverse direction; thus, they have the lowest transverse K_{eff} of 4.7–7.2 with mean 5.9 m/d.

The vertical K_{eff} (<0.05 m/d) is 2–3 orders of magnitude less than horizontal values in Figure 7c compared to 5–15 m/d in Figures 7a and 7b). The flow in the vertical direction relates to the sand geobody thickness. The Pirojpur site has the thinnest geobodies (Table 2); thus, the vertical K_{eff} of Pirojpur models (~3.3×10^{-4} m/d) is significantly lower than the Barisal K_{eff} (~1.5×10^{-2} m/d) and Khulna sites (~5.5×10^{-3} m/d) for both object-based and SIS models. Barisal sinusoid (4.2×10^{-3} to 3.2×10^{-2} with mean of 1.5×10^{-2} m/d) and ellipsoid models (5.3×10^{-3} to 3.7×10^{-3} with mean of 1.6×10^{-2} m/d) show higher variability than the SIS models (3.1×10^{-3} to 2.8×10^{-2} with mean of 8.7×10^{-3} m/d). A possible reason is that the random geobody stacking in object-based simulations may cause occasional large vertical sand connections. The vertical sand distribution is based on the channel thickness in the object-based models, which is similar to the SIS models, thus the vertical K_{eff} of object-based models and SIS models are not significantly different.

Transport behavior is also influenced by the geometry of heterogeneity. *Contaminated volume* in the longitudinal and transverse directions shows a similar result as the K_{eff}, indicating that the effect of geologic structure on the general transport behavior (nonpreferential) is similar to the flow behavior (Figures 7d and 7e). *Farthest contamination extent* represents preferential transport behavior (Figures 7f and 7g). In the longitudinal direction, preferential transport is not significantly different among the different conceptualizations, with a *farthest contamination extent* of 7,000–8,000 m except for Barisal ellipsoid models (4,100–7,700 m with mean of 6,400 m) (Figure 7f),

Accepted Manuscript
Version of Record at: https://doi.org/10.1029/2022JF006775

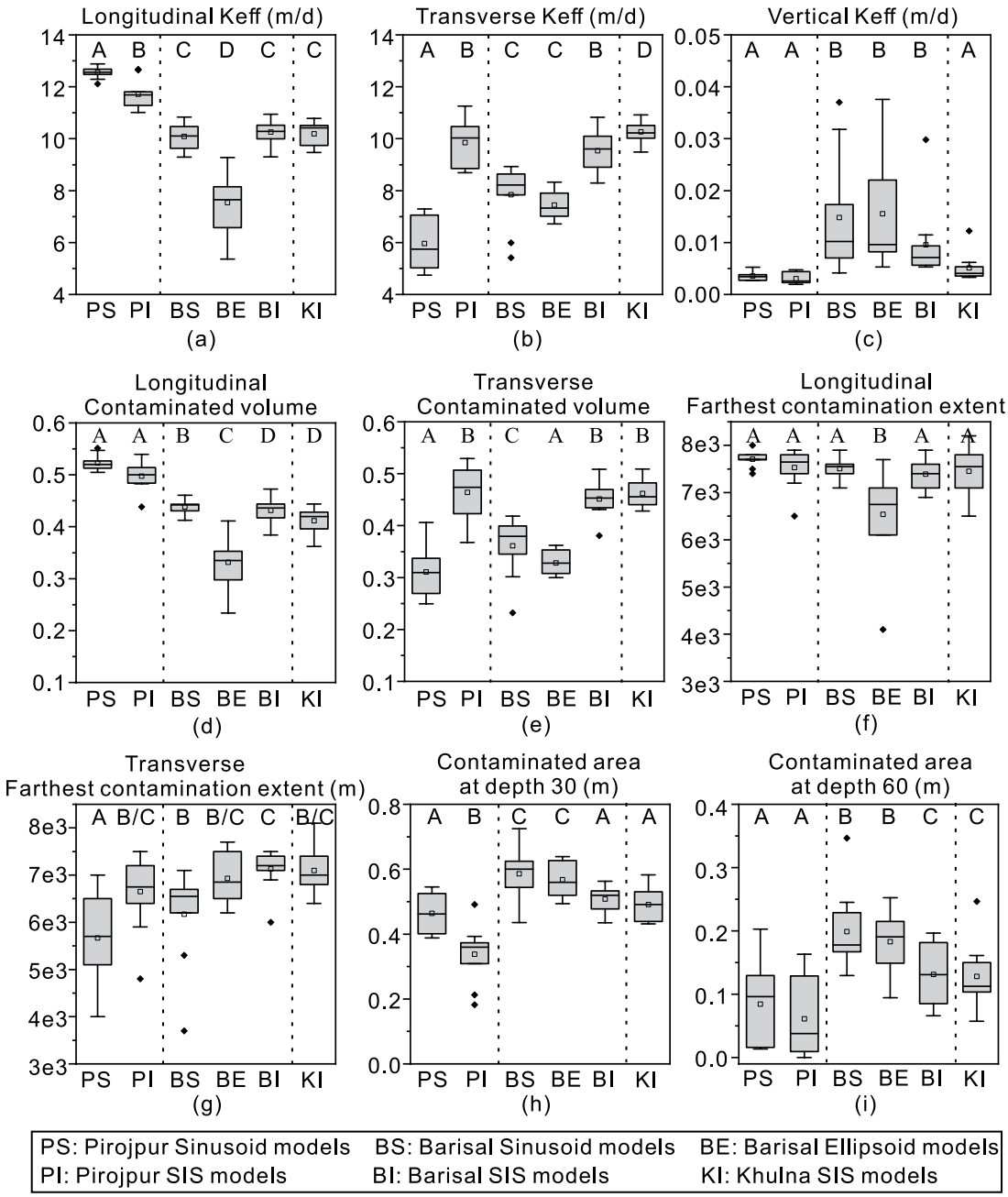

Figure 7. Flow and transport simulation results: (a–c) are effective hydraulic conductivity in three directions. (d, e) are contaminated volume in the longitudinal and transverse directions. (f, g) are farthest contamination extent in the longitudinal and transverse directions. (h, i) are contaminated areas at depths of 30 and 60 m. Labels above each box represent the result of the two-sample *t*-test; the same label means that two groups of data are not statistically different, while different labels indicate that two groups of data are significantly different (p-value <0.05). "A/B" indicates this group of data is insignificantly different compared to data labeled with "A" or "B."

which are less connected. However, in the transverse direction, Barisal ellipsoid models have a greater *farthest contamination extent* (6,200–7,700 with mean of 7,000 m) than other object-based models (4,000–7,100 m with mean of 5,700 m) (Figure 7g). Vertical contamination is demonstrated by *contaminated area at* 30 m and *contaminated area at* 60 m (Figures 7h and 7i). These metrics show that the vulnerability to vertical contamination predicted by SIS models is different from the one predicted by object-based models except *contaminated area at* 60 m of the Pirojpur site. Generally, the Pirojpur site is less vulnerable to vertical contamination than the Barisal and Khulna sites (Figures 7h and 7i).

Accepted Manuscript
Version of Record at: https://doi.org/10.1029/2022JF006775

5. Discussion

This study demonstrates that surface information can be used to improve both the subsurface conceptualization and predictions of flow and transport, indicating a linkage between fluvial geomorphology and subsurface heterogeneity. We demonstrate a methodology to incorporate this surface information quantitatively into models of subsurface architecture using object-based geostatistical methods in which geobody geometries are derived from surface channel information. The results show that three of the object-based models fit well with the field measurements in the active delta (Figure 5 and Table 3), and that the different geometrical conceptualizations derived from surface characteristics are distinguishable using dense lithologic data. In typical systems where such dense lithologic data are unavailable, surface information may be invaluable in developing quantitative models of the subsurface and predicting groundwater flow and solute transport. This method demonstrates the opportunity to take advantage of abundant and accessible surface data from satellite or other sources, potentially overcoming the typical challenge of scarce subsurface data.

We demonstrate the use of surface features using two geometry types—channels and ellipsoids—that are common conceptualizations for deltaic systems. This idea may be extended to other systems in which surface features can be identified in subsurface architecture, such as fluvial (e.g., van Dijk et al., 2016a), volcanic (e.g., Kreyns et al., 2020), or fractured (Schuite et al., 2015) systems. In our analysis, we limit the modeling to single objects, but future work may incorporate multiple objects, which would likely be appropriate in our Barisal site, for example, where both sinusoidal and ellipsoid models fit the data. The geostatistical approach could also be extended by incorporating an understanding of the kinematics of a system—how channels move at the surface relative to previous locations. This could be incorporated into object-based modeling by specifying object affinity, or how likely channels are to be close to or far from other channels. Other geostatistical techniques that are able to simulate continuous geobodies, such as multiple-point geostatistics, could also be employed (Hermans, 2014; Michael et al., 2010; Strebelle & Journel, 2001).

The comparison of flow simulation with object-based versus variogram-based (SIS) models shows that these two approaches represent the subsurface quite differently in terms of conducting groundwater flow. This is true even though the SIS simulations are based on variograms derived from densely distributed data. In the straight-river system, relative to the object-based models, the variogram-based models underestimate the rate of flow and transport along the river axis and overestimate rates across the river axis. The opposite situation may occur in meandering channel systems, and contaminants may move more slowly through high-tortuosity sand channels or point-bar deposits. Similarly, in the vertical direction, deeper channels may be more likely to connect, thus creating more fast-transport paths to depth. Since we do not have dense flow measurements to compare with these results, we cannot be certain which one is more accurate, and these data would be nearly impossible to obtain. The same is true for solute measurements—even if an extremely dense data set were obtained, complex boundary conditions and reactions would make direct validation nearly impossible. However, the pattern of groundwater flow produced by the object-based model is more consistent with some of the effects discussed earlier in this paper (e.g., rapid flow through connected sands) than in the SIS model. Existing data from the Bengal Delta and other locations have shown that these effects can be critically important in controlling groundwater flow and contamination (e.g., Khan et al., 2019; Mozumder et al., 2020). It follows that the use of surface information can benefit groundwater management. Near large rivers, thick sand bodies may occur, leading to deeper arsenic distributions. Thus, groundwater managers may consider deeper pumping wells for extracting safe water. In contrast, areas with smaller river channels may not support fast vertical transport.

Although its value is supported by field borehole data, this surface-subsurface translation approach has limitations. First, we show in our analysis of the Khulna site that subsurface modeling based on surface information is less effective in an inactive delta setting. There, the fluvial processes and sediment supply that constructed most of the aquifer near Khulna shifted eastward in the late Holocene (Allison et al., 2003), being replaced by tidal channels and a finer-grained sediment supply derived from the nearshore river plume (Rogers et al., 2013). Thus, the tidal channel characteristics at the surface of the modern Khulna region are not similar to those of the fluvially dominated system that deposited the subsurface sediment. Therefore, incorporation of surface information for subsurface simulation should be limited to systems in which the active depositional processes are similar to those that deposited the aquifer sediments. The approach may be ineffective in mature deltas, or at depths in which sediments were deposited under a different set of external forcings or allogenic processes. Second, we directly use the parameters of surface features and then stochastically arrange features in the subsurface model, which carries

Accepted Manuscript
Version of Record at: https://doi.org/10.1029/2022JF006775

the assumption that in active deltas, the depositional processes and boundary conditions that created the aquifer are the same as those acting on the surface. This neglects changes in climate, sediment load, and neo-tectonics, for example, Therefore, this method is best applied to shallow strata such that the fluvial processes at the time of deposition were similar to current processes. Furthermore, anthropogenic modifications in the past centuries may have changed the surface morphology and sediment supply; these factors should be considered when applying this method.

At a larger scale of the delta, the influence of the surface environment on the subsurface is also evident. More sand-mud shifts occur in the downstream and near-river regions, an observation that may result from multiple factors and warrants future study. Among the factors that may contribute to the observed downstream increase in aquifer mud fraction and number of sand-mud shifts are fining of the fluvial sediment load through mass extraction (Paola & Martin, 2012), changes in driving forces such as river channel migration, subsidence, tidal effects, and anthropogenic modifications (Hanebuth et al., 2013; Jarriel et al., 2020; Karpytche et al., 2018; Wilson & Goodbred, 2015), and stratigraphic bias from nonuniform channel occupation (Grimaud et al., 2017) or preservation effects (Straub & Esposito, 2013). Short-timescale channel migration can be directly observed from Landsat in the last 30 years (Jarriel et al., 2020, 2021), indicating an active depositional environment that promotes frequent sand-mud shifts, consistent with our data. However, for these surface dynamics and sand-mud switches to be reflected in the deeper aquifer sediments, as they are near Barisal and the modern river, they must be preserved in the stratigraphic record. Such preservation is strongly influenced by larger-scale patterns of river avulsion and burial timescales set by sedimentation and subsidence (e.g., Reitz et al., 2015). In all, our results show that predicting subsurface aquifer properties from land-surface morphology is possible, but also that this approach may be complicated by the implicit integration of processes that may be nonuniform or nonsteady and operating at differing scales.

6. Conclusions

The aim of this study was to explore the applicability of using land surface characteristics, which are readily measured, to predict subsurface structure, groundwater flow, and solute transport, which are difficult to measure directly. Based on analysis of an extensive set of lithologic data in the Bengal Delta and simulations of subsurface permeability distributions guided by the surface channel geometry, we find that:

1. At the large scale of the Bengal Delta, sand proportion tends to decrease seaward, and there are more sediment shifts (between sand and clay) near major rivers and estuaries in the active delta. These results demonstrate the potential to use the position within a delta when predicting subsurface architecture.
2. Information obtained from surface channel networks can be used to develop models of subsurface heterogeneity that are consistent with lithologic data, indicating a linkage between surface features and subsurface structure in actively developing deltas. In the active delta with relatively straight rivers (Pirojpur site), the conceptualization of slightly sinuous channel geobodies fits well with subsurface lithologic field measurements. In the active delta with meandering rivers (Barisal site), both a tortuous channel conceptualization and a lower-ellipsoid conceptualization from surface data are consistent with field measurements. Field data in the inactive, mature delta (Khulna site) are not consistent with models generated from surface information.
3. The geometry of subsurface features, as derived from surface information, is critical for the prediction of groundwater flow and contaminant transport. Horizontal flow and transport are influenced by the geobody connections and the flow direction relative to the geobody extent, and vertical transport is primarily influenced by the geobody thickness. Channel connections and disconnections are important in mediating groundwater flow; these cannot be modeled without explicitly accounting for the geometry and spatial arrangement of channel bodies.

These findings demonstrate that in areas with active sedimentation, geomorphological characteristics on the land surface can be critical sources of information that, in addition to other lithological and geophysical data, can be used to develop models of subsurface heterogeneity that enable more accurate prediction of contaminant migration in groundwater systems.

Data Availability Statement

Simulation of groundwater flow is conducted using MODFLOW (Harbaugh, 2005). Solute transport is simulated by MT3DMS (Zheng & Wang, 1999). Lithologic data obtained in this work and example numerical model input files are available at (Xu, 2022): https://doi.org/10.4211/hs.22d8fe3a93e14d26a2477fa9406a8eba.

Accepted Manuscript
Version of Record at: https://doi.org/10.1029/2022JF006775

Acknowledgments
The authors thank University of Barisal Department of Geology and Mining Professor Alamgir Hosain and students Md Syful Islam and Nayon Islam, University of Dhaka Department of Geology students Mohammad Anisur Rahman Rana, Golam Muktadir, Abu Saeed Arman, Mohammad Tawhidur Rahman Tushar, Md. Ayatulla Al Galib, and Sontu Ram Ray for their invaluable assistance in the field. We also acknowledge support from the US National Science Foundation via EAR-1719670/EAR-1719638 and Fundamental Research Funds for the Central Universities, Grant 2682022CX036.

References

Ahmad, T. (2014). A study on river bank protection works for the Baleshwar River in Pirojpur district (Master's thesis). Bangladesh University of Engineering and Technology.

Alam, M., Alam, M. M., Curray, J. R., Chowdhury, M. L. R., & Gani, M. R. (2003). An overview of the sedimentary geology of the Bengal Basin in relation to the regional tectonic framework and basin-fill history. *Sedimentary Geology*, *155*(3–4), 179–208. https://doi.org/10.1016/S00370738(02)00180-X

Allison, M. A., Khan, S. R., Goodbred, S. L., & Kuehl, S. A. (2003). Stratigraphic evolution of the late Holocene Ganges–Brahmaputra lower delta plain. *Sedimentary Geology*, *155*(3–4), 317–342. https://doi.org/10.1016/S0037-0738(02)00185-9

Allison, M. A., Kuehl, S. A., Martin, T. C., & Hassan, A. (1998). The importance of floodplain sedimentation for river sediment budgets and terrigenous input to the oceans: Insights from the Brahmaputra–Jamuna River. *Geology*, *26*(2), 175–178. https://doi.org/10.1130/00917613(1998)026<0175:IOFPSF>2.3.CO;2

Atker, J., Sarker, M. H., Popescu, I., & Roelvink, D. (2016). Evolution of the Bengal Delta and its prevailing processes. *Journal of Coastal Research*, *32*(5), 1212–1226. https://doi.org/10.2112/JCOASTRES-D-14-00232.1

Auerbach, L. W., Goodbred, S. L., Mondal, D. R., Wilson, C. A., Ahmed, K. R., Roy, K., et al. (2015). Flood risk of natural and embanked landscapes on the Ganges–Brahmaputra tidal delta plain. *Nature Climate Change*, *5*(2), 153–157. https://doi.org/10.1038/nclimate2472

Ayers, J. C., Goodbred, S., George, G., Fry, D., Benneyworth, L., Hornberger, G., et al. (2016). Sources of salinity and arsenic in groundwater in southwest Bangladesh. *Geochemical Transactions*, *17*(1), 4. https://doi.org/10.1186/s12932-016-0036-6

Bangladesh Bureau of Statistics. (2011). *Bangladesh population and Housing Census 2011 socio-economic and demographic report national series, volume—4*. Bangladesh Bureau of Statistics, Statistics Division.

Bangladesh Bureau of Statistics. (2021). Bangladesh MICS 2019: Water quality thematic report. Retrieved from https://psb.gov.bd/policies/wqtr2019.pdf

Barua, D. K., Kuehl, S. A., Miller, R. L., & Moore, W. S. (1994). Suspended sediment distribution and residual transport in the coastal ocean off the Ganges-Brahmaputra river mouth. *Marine Geology*, *120*(1–2), 41–61. https://doi.org/10.1016/0025-3227(94)90076-0

Bhattacharya, J. P. (2011). Practical problems in the application of the sequence stratigraphic method and key surfaces: Integrating observations from ancient fluvial–deltaic wedges with quaternary and modelling studies. *Sedimentology*, *58*(1), 120–169. https://doi.org/10.1111/j.1365-3091.2010.01205.x

Bricheno, L. M., Wolf, J., & Sun, Y. (2021). Saline intrusion in the Ganges-Brahmaputra-Meghna megadelta. *Estuarine, Coastal and Shelf Science*, *252*, 107246. https://doi.org/10.1016/j.ecss.2021.107246

BWDB. (2011). *Rivers of Bangladesh* (2nd ed.). Bangladesh Water Development Board. (p. 341).

BWDB. (2013). *Hydro-geological study and mathematical modelling to identify sites for installation of observation well nests, selection of model boundary, supervision of pumping test, slug test, assessment of different hydro-geological parameters, collection and conduct chemical analysis of surface water and groundwater* (Vol. 2). Bangladesh Water Development Board, The Climate Change Trust Fund Project.

Caers, J. (2000). *Direct sequential indicator simulation*. Stanford University.

Colombera, L., & Mountney, N. P. (2021). Influence of fluvial crevasse-splay deposits on sandbody connectivity: Lessons from geological analogues and stochastic modelling. *Marine and Petroleum Geology*, *128*, 105060. https://doi.org/10.1016/j.marpetgeo.2021.105060

Colombera, L., Mountney, N. P., Russel, C. E., Shier, M. N., & McCaffrey, W. D. (2017). Geometry and compartmentalization of fluvial meander-belt reservoirs at the bar-form scale: Quantitative insight from outcrop, modern and subsurface analogues. *Marine and Petroleum Geology*, *82*, 35–55. https://doi.org/10.1016/j.marpetgeo.2017.01.024

Colombera, L., Yan, N., McCormick-Cox, T., & Mountney, N. P. (2018). Seismic-driven geocellular modeling of fluvial meander-belt reservoirs using a rule-based method. *Marine and Petroleum Geology*, *93*, 553–569. https://doi.org/10.1016/j.marpetgeo.2018.03.042

Deutsch, C., & Tran, T. (2002). Fluvsim: A program for object-based stochastic modeling of fluvial depositional systems. *Computers & Geosciences*, *28*(4), 525–535. https://doi.org/10.1016/S0098-3004(01)00075-9

Deutsch, C. V., & Wang, L. (1996). Hierarchical object-based geostatistical modeling of fluvial reservoirs. In *Paper SPE 36514 presented at annual technical conference and exhibition*. Society of Petroleum Engineers.

DevCon-DPM-KPL. (2013). Feasibility study for Bekutia bridge over Kocha river on Perojpur-Jhalokathi road.

Donselaar, M. E., & Overeem, I. (2008). Connectivity of fluvial point-bar deposit: An example from the Miocene Huesca fluvial fan, Ebro Basin, Spain. *AAPG Bulletin*, *92*(9), 1109–1129. https://doi.org/10.1306/04180807079

DPHEJICA. (2010). *Borelog data book*. Tech. Rep. Department of Public Health Engineering and Japan International Cooperation Agency.

EPA. (2009). National primary drinking water regulations. 54 total coliforms (including fecal coliforms and E. Coli).

Ghosh, S. (2020). Barishal river port: Plastic waste slows down dredging work. Retrieved from https://www.thedailystar.net/city/news/plastic-waste-slows-down-dredging-work-1997489

Goodbred, S. L. (2020). Personal communication.

Goodbred, S. L., & Kuehl, S. A. (1998). Floodplain processes in the Bengal Basin and the storage of Ganges–Brahmaputra river sediment: An accretion study using 137Cs and 210Pb geochronology. *Sedimentary Geology*, *121*(3–4), 239–258. https://doi.org/10.1016/S0037-0738(98)00082-7

Goodbred, S. L., & Kuehl, S. A. (2000). The significance of large sediment supply, active tectonism, and eustasy on margin sequence development: Late Quaternary stratigraphy and evolution of the Ganges–Brahmaputra delta. *Sedimentary Geology*, *133*(3–4), 277–248. https://doi.org/10.1016/S0037-0738(00)00041-5

Goodbred, S. L., Kuehl, S. A., Steckler, M. S., & Sarker, M. H. (2003). Controls on facies distribution and stratigraphic preservation in the Ganges–Brahmaputra delta sequence. *Sedimentary Geology*, *155*(3–4), 301–316. https://doi.org/10.1016/S0037-0738(02)00184-7

Goodbred, S. L., Paolo, P. M., Ullah, M. S., Pate, R. D., Khan, S. R., Kuehl, S. A., et al. (2014). Piecing together the Ganges-Brahmaputra-Meghna River delta: Use of sediment provenance to reconstruct the history and interaction of multiple fluvial systems during Holocene delta evolution. *Geological Society of America Bulletin*, *126*(11), 1495–1510. https://doi.org/10.1130/B30965.1

Gouw, M. J., & Hijma, M. P. (2022). From apex to shoreline: Fluvio-deltaic architecture for the Holocene Rhine–Meuse delta, The Netherlands. *Earth Surface Dynamics*, *10*(1), 43–64. https://doi.org/10.5194/esurf-10-43-2022

Grall, C., Steckler, M. S., Pickering, J. L., Goodbred, S. L., Sincavage, R., Paola, C., et al. (2018). A base-level stratigraphic approach to determining Holocene subsidence of the Ganges–Meghna–Brahmaputra Delta plain. *Earth and Planetary Science Letters*, *499*, 23–36. https://doi.org/10.1016/j.epsl.2018.07.008

Grimaud, J. L., Ors, F., Lemay, M., Cojan, I., & Rivoirard, H. (2022). Preservation and completeness of fluvial meandering deposits influenced by channel motions and overbank sedimentation. *Journal of Geophysical Research: Earth Surface*, *127*(5), e2021JF006435. https://doi.org/10.1029/2021JF006435

Grimaud, J. L., Paola, C., & Ellis, C. (2017). Competition between uplift and transverse sedimentation in an experimental delta. *Journal of Geophysical Research: Earth Surface*, *122*(7), 1339–1354. https://doi.org/10.1002/2017JF004239

Haldorsen, H. H., & Lake, L. W. (1984). A new approach to shale management in field-scale models. *SPE Journal*, *24*(04), 447–457. https://doi.org/10.2118/10976-PA

Hanebuth, T. J. J., Kudrass, H. R., Linstädter, J., Islam, B., & Zander, A. M. (2013). Rapid coastal subsidence in the central Ganges-Brahmaputra Delta (Bangladesh) since the 17th century deduced from submerged salt-producing kilns. *Geology*, *41*(9), 987–990. https://doi.org/10.1130/G34646.1

Harbaugh, A. W. (2005). *MODFLOW-2005, the US geological survey modular groundwater model: The groundwater flow process*. US Department of the Interior, USGS Reston.

Hariharan, J., Xu, Z., Michael, H. A., Paola, C., Steel, E., & Passalacqua, P. (2021). Constraining subsurface properties from surface information in river deltas—Part 1: Relating surface and subsurface geometries. *Water Resources Research*, *57*(8), e2020WR029282. https://doi.org/10.1029/2020WR029281

Hermans, T. J. (2014). Integration of near-surface geophysical, geological and hydrogeological data with multiple-point geostatistics in alluvial aquifers (Doctoral dissertation). University of Liege.

Hoque, M. A., Burgess, W. G., & Ahmed, K. M. (2017). Integration of aquifer geology, groundwater flow and arsenic distribution in deltaic aquifers—A unifying concept. *Hydrological Processes*, *31*(11), 2095–2109. https://doi.org/10.1002/hyp.11181

Hoque, M. A., McArthur, J. M., & Sikdar, P. K. (2012). The palaeosol model of arsenic pollution of groundwater tested along a 32 km traverse across West Bengal, India. *Science of the Total Environment*, *431*, 157–165. https://doi.org/10.1016/j.scitotenv.2012.05.038

Hoque, M. A., McArthur, J. M., & Sikdar, P. K. (2014). Sources of low-arsenic groundwater in the Bengal Basin: Investigating the influence of the last glacial maximum palaeosol using a 115-km traverse across Bangladesh. *Hydrogeology Journal*, *22*(7), 1535–1547. https://doi.org/10.1007/s10040-014-1139-8

Hosono, T., Nakano, T., Shimizu, Y., Onodera, S. I., & Taniguchi, M. (2011). Hydrogeological constraint on nitrate and arsenic contamination in Asian metropolitan groundwater. *Hydrological Processes*, *25*(17), 2742–2754. https://doi.org/10.1002/hyp.8015

Islam, S. N., & Gnauck, A. (2008). Mangrove wetland ecosystems in Ganges–Brahmaputra delta in Bangladesh. *Frontiers of Earth Science in China*, *2* (4), 439–448. https://doi.org/10.1007/s11707-008-0049-2

Jarriel, T., Isikdogan, L. F., Bovik, A., & Passalacqua, P. (2020). System wide channel network analysis reveals hotspots of morphological change in anthropogenically modified regions of the Ganges Delta. *Scientific Reports*, *10*(1), 12823. https://doi.org/10.1038/s41598-020-69688-3

Jarriel, T., Swartz, J. M., & Passalacqua, P. (2021). Global rates and patterns of channel migration in river deltas. *Proceedings of the National Academy of Sciences of the United States of America*, *118*, e2103178118. https://doi.org/10.1073/pnas.2103178118

JICA. (1999). The study on construction of the bridge over the river rupsa in Khulna (Phase I).

Journel, A. G., & Alabert, F. G. (1988). Focusing on spatial connectivity of extreme-valued attributes: Stochastic indicator models of reservoir heterogeneities. *AAPG Bulletin*, *73*(3), 23–26.

Juang, K., Chen, Y., & Lee, D. (2004). Using sequential indicator simulation to assess the uncertainty of delineating heavy-metal contaminated soils. *Environmental Pollution*, *127*(2), 229–238. https://doi.org/10.1016/j.envpol.2003.07.001

Karpytche, M., Ballu, V., Krien, Y., Becker, M., Goodbred, S., Spada, G., et al. (2018). Contributions of a strengthened early Holocene monsoon and sediment loading to present-day subsidence of the Ganges-Brahmaputra Delta. *Geophysical Research Letters*, *45*(3), 1433–1442. https://doi.org/10.1002/2017GL076388

Khan, M. R., Koneshloo, M., Knappett, P. S. K., Ahmed, K. M., Bostick, B. C., Mailloux, B. J., et al. (2016). Megacity pumping and preferential flow threaten groundwater quality. *Nature Communications*, *7*(1), 12833. https://doi.org/10.1038/ncomms12833

Khan, M. R., Michael, H. A., Nath, B., Huhmann, B. L., Harvey, C. F., Mukherjee, A., et al. (2019). High-arsenic groundwater in the southwestern Bengal Basin caused by a lithologically controlled deep flow system. *Geophysical Research Letters*, *46*(22), 13062–13071. https://doi.org/10.1029/2019GL084767

Kreyns, P., Geng, X., & Michael, H. A. (2020). The influence of connected heterogeneity on groundwater flow and salinity distributions in coastal volcanic aquifers. *Journal of Hydrology*, *586*, 124863. https://doi.org/10.1016/j.jhydrol.2020.124863

LGEDBRGM. (2005). *Groundwater resources & hydro-geological investigations in and around Khulna city*. Local Government Engineering Department.

Liang, M., Voller, V. R., & Paola, C. (2015). A reduced-complexity model for river delta formation—Part 1: Modeling deltas with channel dynamics. *Earth Surface Dynamics*, *3*(1), 67–86. https://doi.org/10.5194/esurf-3-67-2015

Liang, M., Voller, V. R., & Paola, C. (2016). Quantifying the patterns and dynamics of river deltas under conditions of steady forcing and relative sea level rise. *Journal of Geophysical Research: Earth Surface*, *121*(2), 465–496. https://doi.org/10.1002/2015JF003653

Maharaja, A. (2008). TiGenerator: Object-based training image generator. *Computers & Geosciences*, *34*(12), 1753–1761. https://doi.org/10.1016/j.cageo.2007.08.012

McArthur, J. M., Nath, B., Banerjee, D. M., Purohit, R., & Grassineau, N. (2011). Palaeosol control on groundwater flow and pollutant distribution: The example of arsenic. *Environmental Science & Technology*, *45*(4), 1376–1383. https://doi.org/10.1021/es1032376

Miall, A. (2014). *Fluvial depositional systems*. Springer Geology.

Michael, H. A., & Khan, M. R. (2016). Impacts of physical and chemical aquifer heterogeneity on basin-scale solute transport: Vulnerability of deep groundwater to arsenic contamination in Bangladesh. *Advances in Water Resources*, *98*, 147–158. https://doi.org/10.1016/j.advwatres.2016.10.010

Michael, H. A., Li, H., Boucher, A., Sun, T., Caers, J., & Gorelick, S. M. (2010). Combining geologic-process models and geostatistics for conditional simulation of 3-D subsurface heterogeneity. *Water Resources Research*, *46*(5), W05527. https://doi.org/10.1029/2009WR008414

Michael, H. A., & Voss, C. I. (2008). Evaluation of the sustainability of deep groundwater as an arsenic-safe resource in the Bengal Basin. *Proceedings of the National Academy of Sciences of United States of America*, *105*(25), 8531–8536. https://doi.org/10.1073/pnas.0710477105

Mihajlov, I., Mozumder, M. R. H., Bostick, B. C., Stute, M., Mailloux, B. J., Knappett, P. S. K., et al. (2020). Arsenic contamination of Bangladesh aquifers exacerbated by clay layers. *Nature Communications*, *11*(1), 2244. https://doi.org/10.1038/s41467-020-16104-z

Milliman, J. D., & Syvitski, J. P. M. (1992). Geomorphic/tectonic control of sediment discharge to the ocean: The importance of small mountainous rivers. *The Journal of Geology*, *100*(5), 525–544. https://doi.org/10.1086/629606

Mozumder, M. R. H., Michael, H. A., Mihajlov, I., Khan, M. R., Knappett, P. S. K., Bostick, B. C., et al. (2020). Origin of groundwater arsenic in a rural Pleistocene aquifer in Bangladesh depressurized by distal municipal pumping. *Water Resources Research*, *55*(7), e2020WR027178. https://doi.org/10.1029/2020WR027178

Naus, F. L., Schot, P., Groen, K., Ahmed, K. M., & Griffioen, J. (2019). Groundwater salinity variation in Upazila Assasuni (southwestern Bangladesh), as steered by surface clay layer thickness, relative elevation and present-day land use. *Hydrology and Earth System Sciences*, *23*(3), 1431–1451. https://doi.org/10.5194/hess-23-1431-2019

Neumann, R. B., Ashfaque, K. N., Badruzzaman, A. B. M., Ashraf Ali, M., Shoemaker, J. K., & Harvey, C. F. (2010). Anthropogenic influences on groundwater arsenic concentrations in Bangladesh. *Nature Geoscience*, *3*(1), 46–52. https://doi.org/10.1038/ngeo685

Paola, C., & Martin, J. M. (2012). Mass-balance effects in depositional systems. *Journal of Sedimentary Research*, *82*(6), 435–450. https://doi.org/10.2110/jsr.2012.38

Passalacqua, P., Lanzoni, S., Paola, C., & Rinaldo, A. (2013). Geomorphic signatures of deltaic processes and vegetation: The Ganges-Brahmaputra-Jamuna case study. *Journal of Geophysical Research: Earth Surface*, *118*(3), 1838–1849. https://doi.org/10.1002/jgrf.20128

Pathak, P., Ghosh, P., Banerjee, S., Chatterjee, R. S., Muzakkira, N., Sikdar, P. K., et al. (2022). Relic surface water (clay-pore water) input triggers arsenic release into the shallow groundwater of Bengal aquifers. *Journal of Earth System Science*, *131*(2), 80. https://doi.org/10.1007/s12040-022-01819-y

Pickering, J. L., Goodbred, S. L., Reitz, M. D., Hartzog, T. R., Mondal, D. R., & Hossain, M. S. (2014). Late Quaternary sedimentary record and Holocene channel avulsions of the Jamuna and Old Brahmaputra River valleys in the upper Bengal delta plain. *Geomorphology*, *227*, 123–136. https://doi.org/10.1016/j.geomorph.2013.09.021

Polizzotto, M. L., Kocar, B. D., Benner, S. G., Sampson, M., & Fendorf, S. (2008). Near-surface wetland sediments as a source of arsenic release to ground water in Asia. *Nature*, *454*(7203), 505–508. https://doi.org/10.1038/nature07093

Pyrcz, M., & Deutsch, C. V. (2014). *Geostatistical reservoir modeling* (2nd ed.). Oxford University Press.

Rasheed, S., Siddique, A., Sharmin, T., Hasan, A., Hanifi, S., Iqbal, M., & Bhuiya, A. (2016). Salt intake and health risk in climate change vulnerable coastal Bangladesh: What role do beliefs and practices play? *PLoS One*, *11*(4), e0152783. https://doi.org/10.1371/journal.pone.0152783

Reitz, M. D., Pickering, J. L., Goodbred, S. L., Paola, C., Steckler, M. S., Seeber, L., & Akhter, S. H. (2015). Effects of tectonic deformation and sea level on river path selection: Theory and application to the Ganges-Brahmaputra-Meghna River Delta. *Journal of Geophysical Research: Earth Surface*, *120*(4), 671–689. https://doi.org/10.1002/2014JF003202

Remy, N., Boucher, A., & Wu, J. (2009). *Applied geostatistics with SGeMS: A user's guide*. Cambridge University Press.

Rogers, K. G., Goodbred, S. L., & Mondal, D. R. (2013). Monsoon sedimentation on the "abandoned" tide-influenced Ganges-Brahmaputra delta plain. *Estuarine, Coastal and Shelf Science*, *131*, 297–309. https://doi.org/10.1016/j.ecss.2013.07.014

Rongier, G., Collon, P., & Renard, P. (2017). A geostatistical approach to the simulation of stacked channels. *Marine and Petroleum Geology*, *82*, 318–335. https://doi.org/10.1016/j.marpetgeo.2017.01.027

Schuite, J., Longuevergen, L., Bour, O., Boudin, F., Durand, S., & Lavenant, N. (2015). Inferring field-scale properties of a fractured aquifer from ground surface deformation during a well test. *Geophysical Research Letters*, *42*(24), 10696–10703. https://doi.org/10.1002/2015GL066387

Seifert, D., & Jensen, J. L. (1999). Using sequential indicator simulation as a tool in reservoir description: Issues and uncertainties. *Mathematical Geology*, *31*(5), 527–550. https://doi.org/10.1023/A:1007563907124

Seto, K. C. (2011). Exploring the dynamics of migration to mega-delta cities in Asia and Africa: Contemporary drivers and future scenarios. *Global Environmental Change*, *21S*, S94–S107. https://doi.org/10.1016/j.gloenvcha.2011.08.005

Shammi, M., Rahman, M. M., Bondad, S. E., & Bodrud-Doza, M. (2019). Impacts of salinity intrusion in community health: A review of experiences on drinking water sodium from coastal areas of Bangladesh. *Healthcare*, *7*(1), 50. https://doi.org/10.3390/healthcare7010050

Stahl, M. O., Tarek, M., Yeo, D. C., Badruzzaman, A., & Harvey, C. F. (2014). Crab burrows as conduits for groundwater-surface water exchange in Bangladesh. *Geophysical Research Letters*, *41*(23), 8342–8347. https://doi.org/10.1002/2014GL061626

Steckler, M. S., Oryan, B., Wilson, C. A., Grall, C., Nooner, S. L., Mondal, D. R., et al. (2022). Synthesis of the distribution of subsidence of the lower Ganges-Brahmaputra Delta, Bangladesh. *Earth-Science Reviews*, *224*, 103887. https://doi.org/10.1016/j.earscirev.2021.103887

Straub, K. M., & Esposito, C. R. (2013). Influence of water and sediment supply on the stratigraphic record of alluvial fans and deltas: Process controls on stratigraphic completeness. *Journal of Geophysical Research: Earth Surface*, *118*(2), 625–637. https://doi.org/10.1002/jgrf.20061

Strebelle, S. B., & Journel, A. G. (2001). Reservoir modeling using multiple-point statistics. In *SPE annual technical conference and exhibition*. Louisiana. https://doi.org/10.2118/71324-MS

Syvitski, J. P. M., & Saito, Y. (2007). Morphodynamics of deltas under the influence of humans. *Global and Planetary Change*, *57*(3–4), 261–282. https://doi.org/10.1016/j.gloplacha.2006.12.001

Szabo, S., Brondizio, E., Renard, F. G., Hetrick, S., Nicholls, R. J., Matthews, Z., et al. (2016). Population dynamics, delta vulnerability and environmental change: Comparison of the Mekong, Ganges–Brahmaputra and Amazon delta regions. *Sustainability Science*, *11*(4), 539–554. https://doi.org/10.1007/s11625-016-0372-6

Tasich, C. M. (2012). Effects of tidal fluctuations on a semi-confined aquifer system in southwest Bangladesh. Master's thesis. Vanderbilt University.

van Dijk, W. M., Densmore, A. L., Singh, A., Gupta, S., Sinha, R., Mason, P. J., et al. (2016a). Linking the morphology of fluvial fan systems to aquifer stratigraphy in the Sutlej-Yamuna plain of northwest India. *Journal of Geophysical Research: Earth Surface*, *121*(2), 201–222. https://doi.org/10.1002/2015JF003720

van Dijk, W. M., Densmore, A. L., Singh, R., Sinha, A., & Voller, V. R. (2016b). Reduced-complexity probabilistic reconstruction of alluvial aquifer stratigraphy, and application to sedimentary fans in northwestern India. *Journal of Hydrology*, *541*, 1241–1257. https://doi.org/10.1016/j.jhydrol.2016.08.028

van Engelen, J., Bierkens, M. F. P., Delsman, J. R., & Essink, G. H. P. O. (2021). Factors determining the natural fresh-salt groundwater distribution in deltas. *Water Resources Research*, *57*(1), e2020WR027290. https://doi.org/10.1029/2020WR027290

van Geen, A., Zheng, Y., Goodbred, J., Horneman, A., Aziz, Z., Cheng, Z., et al. (2008). Flushing history as a hydrogeological control on the regional distribution of arsenic in shallow groundwater of the Bengal Basin. *Environmental Science & Technology*, *42*(7), 2283–2288. https://doi.org/10.1021/es702316k

Wilson, C. A., & Goodbred, S. L. (2015). Construction and maintenance of the Ganges-Brahmaputra-Meghna Delta: Linking process, morphology, and stratigraphy. *Annual Review of Marine Science*, *7*(1), 67–88. https://doi.org/10.1146/annurev-marine-010213-135032

Worland, S. C., Hornberger, G. M., & Goodbred, S. L. (2015). Source, transport, and evolution of saline groundwater in a shallow Holocene aquifer on the tidal deltaplain of southwest Bangladesh. *Water Resources Research*, *51*(7), 5791–5805. https://doi.org/10.1002/2014WR016262

Xu, Z. (2022). Surface to subsurface—Bengal delta [Dataset]. HydroShare. https://doi.org/10.4211/hs.22d8fe3a93e14d26a2477fa9406a8eba

Xu, Z., Hariharan, J., Passalacqua, P., Steel, E., Chadwick, A., Paola, C., et al. (2022). Effects of geologic setting on contaminant transport in deltaic aquifers. *Water Resources Research*, *58*(9), e2022WR031943. https://doi.org/10.1029/2022WR031943

Xu, Z., Hariharan, J., Passalacqua, P., Steel, E., Paola, C., & Michael, H. A. (2021). Linking the surface and subsurface in river deltas—Part 2: Relating subsurface geometry to groundwater flow behavior. *Water Resources Research*, *57*(8), e2020WR029281. https://doi.org/10.1029/2020WR029281

Zheng, C., & Wang, P. P. (1999). *MT3DMS: A modular three-dimensional multispecies transport model for simulation of advection, dispersion, and chemical reactions of contaminants in groundwater systems: Documentation and user's guide*. DTIC Document.

References From the Supporting Information

BWDB. (2020). *Bangladesh weather and climate service regional project component-b strengthening hydrological information services and early warning systems*. Bangladesh Water Development Board, Bangladesh Weather and Climate Services Regional Project.